*Desalination and Water Treatment*
www.deswater.com
20 (2010) 253–263
August
1944-3994 / 1944-3986 © 2010 Desalination Publications. All rights reserved.
doi: 10.5004/dwt.2010.1579

# Study and modeling of the separation characteristics of a novel alkali-stable NF membrane

Liming Zhao[a], Wenshui Xia[a]*, Hefei Zhao[b], Jun Zhao[b]

[a]*State Key Laboratory of Food Science and Technology, School of Food Science and Technology, Jiangnan University; 1800, Lihu Avenue, Wuxi City, Jiangsu Province 214122, China*
*Tel. +86 (510) 85919121; Fax +86 (510) 85329057; email: xiaws@jiangnan.edu.cn*
[b]*Hydrochem Engineering (Shanghai) Co., Ltd., 99 JuLi Road, Zhangjiang Hi-Tech Park, Pudong Area, Shanghai 201203, China*

Received 15 October 2009; Accepted in revised form 29 January 2010

**ABSTRACTS**

In this study, we used several methods to examine the membrane structure of a kind of alkali-stable nanofiltration membrane, as well as the effect of pH on its permeability, retention, and structure. A novel alkali-stable nanofiltration membrane was studied. Its retention and flux behavior could be related to its charge, its swelling properties and its pore size distribution. The filtration performed was of uncharged glucose, salt solutions, and caustic sodium solution. A novel artificial neural network-based model was generated to simulate the permeate flux and retention behaviors. Our experimental data were compared with the model outputs. A Spiegler–Kedem model was also examined in this study. Our results showed that the membrane pore diameter was about 0.36 nm, and had a negative surface charge. In addition, the membrane opened significantly at high pH, a finding which can be attributed to the chemical nature of the polymer chains in the membrane skin layer. The correlation factor of the artificial neural network model was 0.9918, which was a little higher than that of Spiegler–Kedem model, indicating that both models are suitable to predict this membrane system.

*Keywords*: Nanofiltration; Structure parameter; Artificial neural networks; Surface charge; Retention; pH dependency

## 1. Introduction

Nanofiltration (NF) membranes represent a class of membranes with the capability to selectively separate low molecular weight solutes. They find application in fields as diverse as the chemical and pharmaceutical industries, bioengineering, environmental protection, water and wastewater treatments, and resource recovery. The chemical stability of existing NF membranes limits their use to rather mild pH and temperature conditions. Many industries generate substantial streams at extreme temperatures and pH, thus creating a demand for NF membranes with a high resistance to extreme conditions. Examples of such streams include alkaline or acidic wastewater from chitin processing, and milk cleaning in place (CIP) discharge.

To meet this demand, a novel NF membrane with increased stability under extreme pH conditions has been developed. For industrial applications, NF membrane properties and flux decline characteristics need to be well-understood; however, few studies have focused on such characterizations.

* Corresponding author.

Nanofiltration separation processes are a combination of sieving and molecular diffusion through the selective layer of the membrane. Surface charge can also play a more important role in NF separation than in other membrane processes. Hence, if two NF membrane surfaces have different surface charge patterns, they are likely to exhibit different ion retentions at different pHs, even if their permeabilities and pore sizes were comparable. The effective separation layer of an NF membrane can be modeled as a three-dimensional network of polymer chains. In this view, NF membranes do not have real pores, but just void spaces inside the polymer chain network. Changes in this void space would clearly impact the membrane permeability and influence the passage of uncharged molecules [1].

The retention by NF membranes of various molecules in solutions at several pHs has been intensively investigated in the last several years [2–9]. Those studies all adopted models of NF behavior that required some characterization of the membranes' physical parameters, such as pore radius, membrane charge and pore dielectric constant. The retentions of charged species, e.g. ions, have been found to depend on the valency, the concentration and chemical nature of the other compounds in solution, and on the membrane surface charge, charge density, and the chemical nature of the groups on the membrane surface. The retention of uncharged species such as organics depends on molecular size and shape, as well as the chemical nature and the hydrophilicity of the compounds [1].

Artificial neural networks (ANN) are widely used to determine connections between input and output data sets, and are used as an alternative to traditional physicochemical models of process behavior. ANN have come to be powerful modeling tools in membrane technology, and much research has been carried out on the modeling, prediction, simulation and process control [10–22] of membrane processes. All of these studies show that neural networks are (i) easy to use, (ii) sufficiently accurate for examining process dynamics, and (iii) computationally efficient tools for modeling various phenomena in membrane science and technology.

The aims of this work were to study the properties and characteristics of the NF membrane exposed to alkali conditions, and to test the NF membrane in the pH range from 7 to 14. We studied not only monovalent salt retention, but also the retention of a small, uncharged organic hydrophilic molecule (glucose).

In this study, ANN and Spiegler–Kedem (SK) models were used to fit and predict the experimental data. In particular, the latter model was able to calculate the σ and $P_s$ for all studied solutes and membrane, while ANN was applied to provide a means of modeling the NF process performance. Flux and retention predictions by both the ANN and SK models were compared. For each experiment, correlation coefficient values were calculated for both ANN and SK models, and analyses of variations and error contributions were made. This is important for understanding the performance of nanofiltration membranes under different conditions. Furthermore, the results facilitate the choice of membranes for specific applications like waste alkali recovery.

## 2. Material and methods

### 2.1. Membrane and equipment

The NF membrane (HDS-04) we studied is a polysulfone-type membrane and is highly resistant to alkali. It can tolerate up to a 20% sodium hydroxide solution or up to a 10% potassium hydroxide solution, according to the manufacturer's instructions. This membrane comprises a triple-layer thin-film composite consisting of a non-woven fabric layer, and an asymmetric porous layer of polysulfone which supports an proprietary ultra-thin selective layer a few tens to a few hundred of nanometers thick. All experiments were carried out using a spiral membrane HDS-04 (Hydrochem, China) with an effective total membrane area of 1.4 $m^2$. The pilot plant for this study was designed by Hydrochem. A Hydra-Cell plunger pump (G10XKCGGHEHB, USA) was used to provide pressure in order to drive the separation. Fig. 1 shows a schematic diagram of the NF pilot plant.

In this study, we conducted experiments in batch mode, with a recirculation of the rententate. A 50 L feed tank included a mixer for homogenation of the feed solution and a heat exchanger for temperature control. Next to the plunger pump was a manometer (PG1) for measuring the pump pressure. Two manometers (PG2 and PG3), placed on either side of the membrane module, measured the pressure drop across the NF membrane. The retentate was recirculated to the feed tank, while the permeate flowed to a downstream reservoir. Retentate

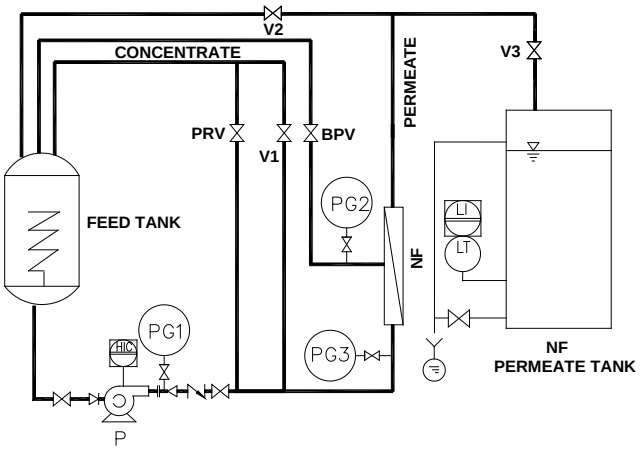


Fig. 1. Schematic diagram of NF pilot plant: P — plunger pump; PG1, PG2, PG3 — manometer; NF — NF membrane module; BPV, V1, V2, V3, PRV — valves.

and bypass valves situated just after PG2 and before PG3 were used to regulate the trans-membrane pressure (TMP). The permeate flux was measured volumetrically with a graduated cylinder.

### 2.2. Chemicals

All chemicals used were of analytical grade. NaCl and glucose were used in filtration runs because they are the compounds relevant to sugar applications and to most retention analyses. The pH was adjusted with 0.1 M sodium hydroxide (NaOH) or potassium hydroxide (KOH). RO-filtered, pure water with a conductivity of less than 1 μS/cm was used in all filtrations.

### 2.3. Nanofilter runs

Filtration experiments to study the retention properties of the studied membrane as a function of the TMP were made using the pilot set-up. Filtrations were conducted at 25°C in total recycle mode, where both the permeate and the concentrate were returned to the feed vessel.

The model solution contained 5% (w/w) glucose in pure water. The volume of the feed tank was about 50 L. Before the filtration of the model solution, the membrane was dipped in 50% ethanol solution for about 5 s. After that, it was flushed with pure water, and installed in the module. Experiments were started by pressurizing the membranes at a pressure of 20 bar for about 10 min. Glucose was then added and samples (about 30 mL) were first collected at the natural pH after 15 min of filtration. After that, the TMP was increased stepwise up to the highest pressure the membrane can endure.

To study the membrane swelling property as a function of pH, glucose or salt was added into the pure water, and the pH was increased stepwise using NaOH (or KOH) and, after reaching the highest pH under study (approximately 13.5), the apparatus was flushed with water. Filtration at each pH was continued for over 2 h and samples were taken after 1h of filtration.

### 2.4. Analysis methods

NaOH was determined by titration of standard hydrochloric acid (HCl). The salt content was analyzed by measuring the chloride ions with ion chromatography or by measuring the sodium ions with atomic absorption spectroscopy.

Glucose was determined by high performance liquid chromatography (HPLC) (Waters 600, USA), under the following conditions: column: Sugarpark 1, 6.5 mmid × 300 mm $Ca^{2+}$ exchange column; liquid phase: pure water; flow rate: 0.4 mL/min; detector: RID, waters 2410; sensitivity: 4; column temperature: 85°C; injection volume: 20 μL. Standard samples of glucose were purchased from Sigma. Samples with a pH higher than 12 were adjusted with 0.1 M HCl to neutrality.

Permeate flux and flow rate were determined with a graduated cylinder and stopwatch.

### 2.5. Calculation of data

The permeate flux through the membrane was calculated using the following equation:

$$J_v = \frac{V}{A_m \cdot t} \tag{1}$$

where $J_v$ is permeate flux, $V$ is the volume of permeate measured by cylinder, $t$ is filtration time, $A_m$ is membrane area.

The TMP was calculated using Eq. (2)

$$\Delta P = \frac{P_{in} + P_{out}}{2} - P_p \tag{2}$$

where $P_{in}$ is inlet pressure of the membrane module, and $P_{out}$ is the outlet pressure of membrane. $P_p$ is the pressure of permeate side.

The gauge pressure was used in this paper, which was equal to the difference value between absolute pressure and atmospheric pressure, and the V2 valve was full opening, hence the gauge pressure of permeate side was zero.

The retentions were calculated as:

$$R = 1 - \frac{C_p}{C_f} \tag{3}$$

where $R$ is retention, $C_p$ is the concentration in the permeate, and $C_f$ is the concentration in the feed.

Data processing and mathematical modeling were carried out using Matlab™ R2007a, a scientific computer program.

## 3. Theories/modeling

### 3.1. NF models

The transport of solute through NF membranes can be described by irreversible thermodynamic models where the membrane is considered as a black box. Kedem and Katchalsky [23] proposed modeling the volume flux $J_v$ through a membrane as given in the following equation:

$$J_v = L_p \cdot (\Delta P - \sigma \cdot \Delta\pi) \tag{4}$$

The flux $J_v$ is related to three membrane parameters: σ, $\Delta\pi$ and $L_p$, where σ, $P_s$ and $L_p$ are the reflection coefficient, the osmosis pressure, and the pure water permeability, respectively. σ depends on the chemical identity of the solute, the solute concentration, and the filter temperature. Its value is approximately equal to the max retention value of membrane. For a single-solute system, σ is a

membrane-specific parameter of the solute. $\Delta\pi$ is related to the concentration of a solution, and it can be neglected if the solution is dilute enough. It can be related via complex Pitzer functions and simply expressed Vant Hoff functions. The combined Vant Hoff expression is as follows:

$$\Delta\pi = R_g \cdot T \cdot \left(C_m - C_p\right) \tag{5}$$

where $C_m$ is the solute concentration on the membrane surface, $C_p$ is concentration in the permeate, and $R_g$ is the ideal gas constant, and $T$ is the temperature.

According to the Hagen–Poiseuille equation, $L_p$ can be expressed as:

$$L_p = \frac{r_p^2}{8 \cdot \mu \cdot \left(\frac{\Delta x}{A_k}\right)} \tag{6}$$

where $\mu$ is the dynamic viscosity, $r_p$ is the theoretical pore radius, $A_k/\Delta x$ is the ratio of membrane porosity to thickness.

Due to concentration polarization on the surface of membrane, the real solute concentration at the membrane surface is different from the bulk concentration. The real concentration of solute rejected by membrane is the surface concentration $C_m$; thus, the real retention ought to be defined by $C_m$ and the permeate concentration $C_p$ as Eq. (7):

$$R = 1 - \frac{C_p}{C_m} \tag{7}$$

where $R$ is the real retention of solute by the membrane, $C_m$ is the solute concentration at the membrane surface, and $C_p$ is the permeate concentration.

Spiegler and Kedem [24] obtained the well-known Spiegler–Kedem (SK) expression for the rejection rate of the solute as a function of the hydrodynamic flux, using an irreversible thermodynamics model. The SK approach is usually applied when no electrostatic interactions exist between membrane and solute. Specifically,

$$R = 1 - \frac{1-\sigma}{1 - \sigma \cdot \exp\left(-J_v \cdot \frac{1-\sigma}{P_s}\right)} \tag{8}$$

where $P_s$ is solute permeability, and $J_v$ the water flux. It can be seen that the rejection rate increases with increasing water flux and at an infinite volume flux reaches a limiting value of $\sigma$. This case applies when the membrane is uncharged, as in reverse osmosis membranes, or when the solute is neutral (organic compounds). Many authors [25–27] have extended this model to the retention of an electrolyte by a charged NF membrane by taking the parameters $\sigma$ and $P_s$ as dependent on the membrane effective charge and on the concentration of solute in the feed.

The above-mentioned parameters $\sigma$ and $P_s$ can be estimated with many models of membrane charge characteristics and structural parameters. Examples include the Teorell–Meyer–Sievers (TMS) model, which has been used to describe ionic transport through charged NF membrane; the steric hindrance pore model (SHP), which takes into account both effects from the steric hindrance of solute and the interaction between solute and pore wall; and electrostatic-steric-hindrance model (ES).

The SHP model gives these expressions for $\sigma$ and $P_s$:

$$\sigma = 1 - H_F \cdot S_F \tag{9}$$

$$P_s = H_D \cdot S_D \cdot D_s \cdot \left(\frac{A_k}{\Delta x}\right) \tag{10}$$

where $D_S$ is the solute diffusivity, and $H_F$ and $H_D$ are, respectively, convection and diffusion steric parameters, related to wall correction factors for the solute. Similarly, $S_F$ and $S_D$ are, respectively, the convection- and diffusion-averaged distribution coefficients for steric effects only.

$$H_F = 1 + \frac{16}{9} \cdot \lambda^2 \tag{11}$$

$$H_D = 1 \tag{12}$$

$$S_F = (1-\lambda)^2 \cdot \left[2 - (1-\lambda)^2\right] \tag{13}$$

$$S_D = (1-\lambda)^2 \tag{14}$$

$$\lambda = \frac{r_s}{r_p} \tag{15}$$

$$\frac{A_k}{\Delta x} = \frac{P_s}{H_D \cdot S_D \cdot D_s} \tag{16}$$

In the SHP model, $\lambda$ is the ratio of the solute radius $r_s$ to the membrane pore radius $r_p$.

### 3.2. *Artificial neural network model*

Over the past few years, artificial neural networks (ANN) have proven to be a useful tool in many engineering applications [28]. The fundamental feature of neural networks is that they are trained, not programmed [12,29]. In theory, a functional relationship between an arbitrary number of input variables to an arbitrary number of output variables can be built by ANN with only two layers (an input, a hidden and an output layer) whose hidden-layer transfer function is nonlinear and whose output-layer transfer function is purely linear. Transfer functions calculate a layer's output from its net input and contain log-sigmoid (logsig), tan-sigmoid (tansig) and pure linear (purlin) functional elements, as shown in Fig. 2.

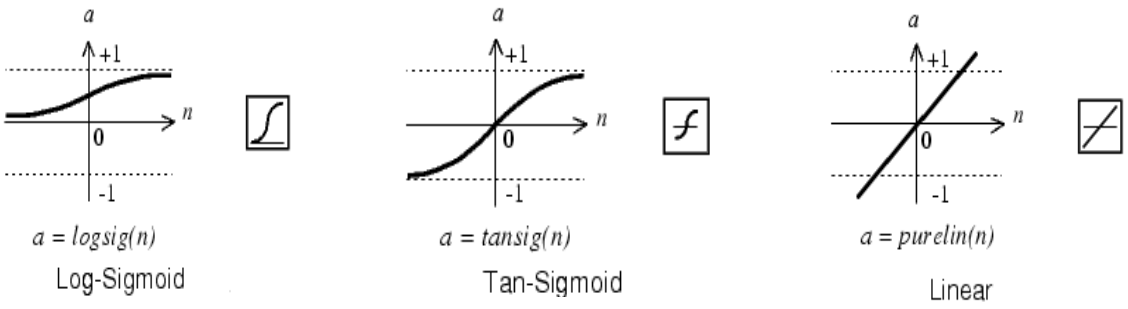


Fig. 2. Transfer functions of ANN.

The successful application of neural networks requires selection of appropriate neural network architecture, and suitable data preprocessing, training and performance evaluation [30].

As can be seen from Fig. 3, we have chosen a feed-forward neural network with two layers. This design is one of the most famous and frequently implemented network types.

Our network architecture comprises an iterative back-propagation (BP) training method because of this method's documented ability to model any function. The input neurons were given the input data (i.e., experimental conditions) and the network gave its outputs (ANN simulation data). If the ANN output was not equal to the experimentally measured outputs, our procedure computed the mean square error between the two values and changed the ANN weights in order to minimize it. These operations were repeated for each input pattern until the total mean square error was minimized.

As can be seen from Fig. 3, the input vector **P** is represented by the solid vertical bar on the left. The dimension of **P** is displayed below the variable as $I^1 \times 1$, indicating that the input is a single vector of $I^1$ elements. These inputs go into the weights matrix $\mathbf{W^1}$ in the hidden layer, which has $I^1$ columns and $S$ rows. A constant 1 enters the neurons as an input and is multiplied by a bias $b_i$ and represented as **b** vector. This vector is summed with the weighted inputs ($\mathbf{W^1}$) to form the net input $\mathbf{n^1}$ vector with $S$ dimensions as seen in Eq. (17):

$$\mathbf{n}^1 = W^1 P + b^1 \tag{17a}$$

$$\mathbf{n}^2 = W^2 a^1 + b^2 \tag{17b}$$

The neurons output vector $\mathbf{a^1}$, with $S^1$ dimensions, is then obtained by applying the transfer function to $\mathbf{n^1}$. The same procedure is repeated in the output layer. The net inputs to the output layer are shown in Eq. (17), while $\mathbf{a^2}$ represents the overall output of the network. This output could be a scalar or a vector, depending on the case under study. There are usually four steps involved in ANN modeling [28].

In this study, we parameterized our data and ANN model using the following notation:
$P_0$: a 2×30 matrix of training samples, where 2 represents independent variables containing the concentration and TMP, or containing the concentration and flux, and where 30 represents 30 combinations of independent variables; $P$: a 2×1 matrix of independent variables; $T_0$: a 1×30 matrix representing the target signal, where 1 represents flux or retention; and where 30 represents 30 experimental dependent variables; $T$: a 1×1 matrix of dependent variables as calculated by ANN simulation, the same as $\mathbf{a^2}$; $\mathbf{W^1}$: a 10×2 weight matrix for the hidden layer; $\mathbf{W^2}$: a 1×10 weight matrix for the outer layer.

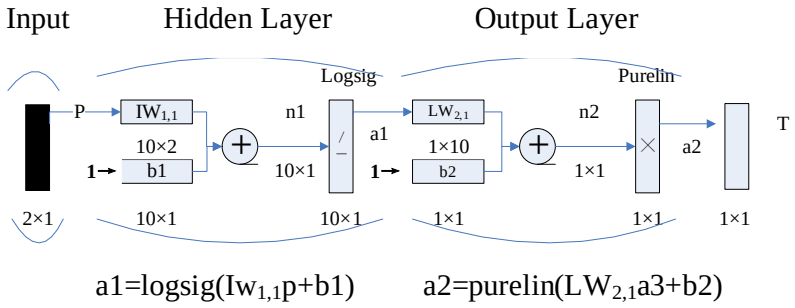


Fig. 3. Architecture of ANN with two layers.

## 4. Results and discussion

### 4.1. Evaluation of membrane structural parameters

Molecular weight cut-off (MWCO) is an empirical parameter usually used to characterize the retention ability of a membrane. It is defined as the molecular weight of an uncharged organic molecule, whose apparent retention is 90% in dilute solution. The retention of uncharged organics by NF membranes is a very important parameter for evaluating membrane separation characteristics. In this study, we used glucose (MW 180 Da) as the solute, at a concentration of 5% (w/w), a pH of 7.1, and a temperature controlled at 23±2.8°C.

As shown in Fig. 4, permeate flux $J_v$ increased linearly with the TMP, with a correlation factor of 0.9993. Because of osmotic pressure, the trend back-extrapolated from the experimental data always has a positive intersect with the $x$-axis. We know from Eq. (3) that the value of $x$-axis intercept is about equal to the osmolality of a solution, because the reflectance ($\sigma$) is close to 1 for high-retention solutes.

As shown in Fig. 5, the permeate flux increases with TMP, as does the membrane retention of glucose, which increases somewhat with TMP until it reaches a plateau. It can be estimated by the definition of MWCO that the MWCO of this NF membrane is less than 180 Da. Model parameters were obtained from fitting to the SK equation, and the reflectance ($\sigma$) of membrane to glucose was found to be 0.9914, with the $P_s$ being 0.0596 L m$^{-2}$ h$^{-1}$. Wang et al. [33] estimated that the Stokes radius of glucose was 0.365 nm and its diffusion coefficient was $0.67\times10^{-9}$ m$^2$ s$^{-1}$. For the SHP model, the NF membrane pore radius was calculated as 0.380 nm and separation layer effective thickness ($\Delta x/A_k$) was calculated as 65.63 nm. The results indicate that the chosen NF membrane exhibits high retention of glucose, and that the theoretical pore radius is a little larger than glucose's Stokes radius. This result also gives confidence that NaOH could permeate completely, while proteins and peptides can be well retained.

### 4.2. Membrane swelling effects of pH

Maintaining the TMP at 25 bar to keep the flux at 25.5 ± 2.1 L m$^{-2}$ h$^{-1}$, we increased the pH of a 5% glucose solution from pH 7.1 in a stepwise fashion, and after 30 min at each pH, we sampled to system to determine the retention and the permeate concentration of the solute. The retention of the membrane to glucose decreased to 0.9792 at pH 13.62 from 0.9913 at pH 7.1, as shown in Fig. 6. In tandem, the flux increased from 23.4 L m$^{-2}$ h$^{-1}$ at pH 7.1 to 27.6 L m$^{-2}$ h$^{-1}$at pH 13.62. Combining the analysis described in Fig. 5 and the SK function, the retention of glucose is predicted to slightly increase with flux in low-flux regimes, or asymptotically approach the reflectance value in high-flux regimes. It can be speculated that flux increases did not contribute to the decrease of retention seen upon increasing the pH.

Manttar et al. [1] studied the effect of pH (pH < 12) on glucose retention in NF and compared many brands of NF membranes (but not anti-alkali NF), and showed that changes in glucose retention with pH were different between the tested NF membranes, nonetheless that retention followed a common, decreasing trend with increasing pH for pHs over 8. Nilsson et al. [32] studied NFT-50 and found that increasing KCl concentrations resulted in decreasing glucose retention at fixed pH values, with the extent of retention decrease being higher at high pH than at low pH. Other workers thought that membrane swelling was the key factor leading to the decreased retention of glucose [31]. The NaOH in solution can not be neglected when pH is over 12. Referring to the results of Nilsson et al., we can speculate that, for alkali-stable NF, the simultaneous increase in pH and ionic strength stemming from increased NaOH concentrations results in membrane swelling at high pHs. Hence, glucose retention decreased due to a swelling-driven increase of the pore radius. This finding can also be obtained from the Hagen–Poiseuille model (H–P), which predicts increasing permeate flux through the membrane in response to an increase in the pore radius.

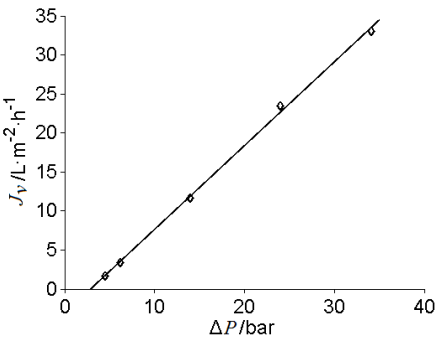


Fig. 4. Permeate flux vs. TMP of the glucose solution. $T$ 23±2.8°C; glucose concentration 5%.

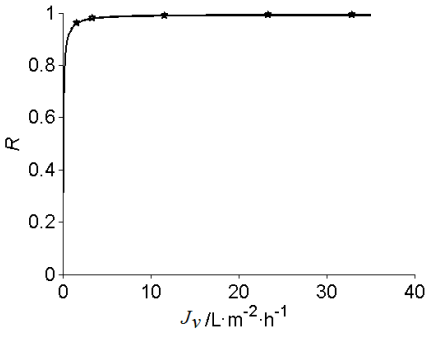


Fig. 5. Permeate flux to glucose retention and permeate flux. $T$ 23±2.8°C; glucose concentration 5%. The TMP can be seen from Fig. 4.

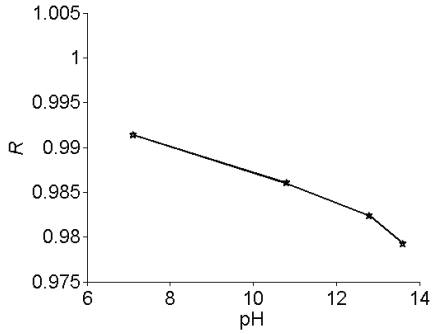


Fig. 6. Retention of glucose as a function of pH at solute concentration of 5%, TMP 25 bar, flux 25.5 ± 2.1 L.m$^{2}$·h$^{-1}$.

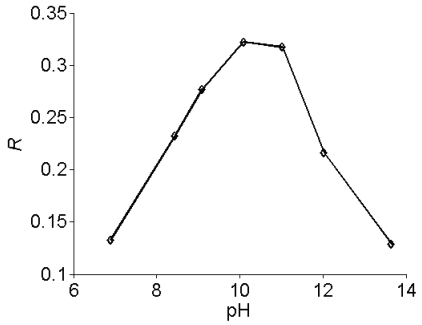


Fig. 7. Effect of pH on $Cl^-$ retention at TMP 25 bar and 25°C at fixed concentration 0.06 mol/L.

### 4.3. Effect of pH on salt retention

The feed pH can affect membrane properties (such as surface charge, hydrophilicity, or porosity) and the speciation of solutes. The effect of pH on salt retention was investigated by filtration of a NaCl solution at a fixed concentration of 0.06 mol/L and at a constant TMP of 25 bar. The pH was adjusted using potassium hydroxide. The retention of $Cl^-$ increased with increasing of pH, tending to a peak value at pH 10, as shown in Fig. 7. The rejection decreased with increasing pH. Compared to glucose retention by this NF membrane, the salt retention was much lower, and the differential between the two values was about 0.7. This result is a strong indication that this membrane is negatively charged. The hydrolysis extent of membrane material increases with increasing pH, leading to increased charging of the membrane surface. That results in the increased exclusion of negative ions from electrolytes by the membrane and thus, in an increase of $Cl^-$ retention at neutral pH. However, the increase of ionic strength due to increasing potassium hydroxide concentrations can not be ignored at high concentrations of potassium hydroxide. The increase in ionic strength compresses the electric double layer and the Debye length ($k^{-1}$) of membrane surface and pore wall reduced.

$$\text{Debye } k^{-1} \propto 1/C^{1/2} \tag{18}$$

where $C$ is the concentration of electrolyte. Increasing ionic strength results in the increasing screening out of charge effects, and thus the electrostatic effect of the membrane becomes weaker. Combined with the analysis of membrane swelling in section 4.2, this fact can explain why $Cl^-$ retention decreases at pH > 10.

### 4.4. Effect of temperature on flux and NaOH retention

Fig. 8 illustrates the changes in flux and solute retention with temperature. It shows that the flux almost linearly increased with increasing temperature, while on the contrary, the NaOH retention by membrane decreased with increasing temperature.

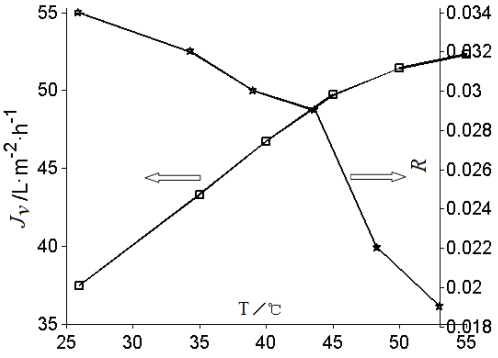


Fig. 8. Effect of temperature on flux of NaOH solution and NaOH retention at certain TMP, $\Delta P$ = 25bar, concentration of NaOH 1.03 mol/L.

The solution viscosity decreases with increasing temperature, and it can be obtained via the HP equation that a temperature increase results in the increasing permeate flux at fixed TMP, while simultaneously, membrane swelling enlarges the pore radius of the membrane, which also contributes to the flux increase. The decrease in NaOH retention can be also explained by membrane swelling.

### 4.5. Effect of TMP and NaOH concentration on flux and NaOH retention

Fig. 9 plots the permeate flux of the investigated membrane at different pressures and NaOH concentrations ranging from 0.244 to 2.651 mol·L$^{-1}$, with samples being collected simultaneously from both sides of membrane. Permeate flux increased with increasing TMP, while it decreased with increasing concentrations of NaOH at the fixed pressures, as shown in Fig. 10. When the NaOH concentration was fixed, the slope of the curves decreased with increasing pressure, which can be explained by the increase in the concentration polarization effect stemming from an increase in permeate flux following a pressure increase. The increased concentration at the membrane

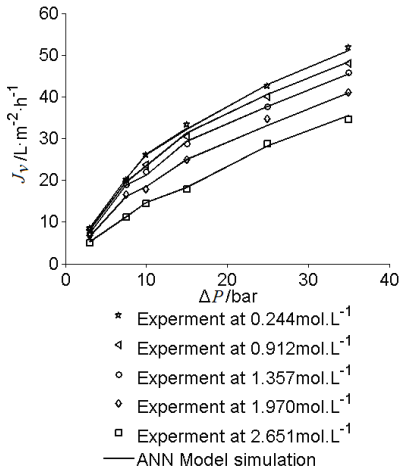


Fig. 9. Permeate flux as a function of TMP and concentration, $R$ = 0.9997.

surface resulted in osmotic pressures at low concentration which were lower than at high TMP. It can be observed that the curve would depart from model predicted values with a fixed slope. Thus, the phenomena where the curve departed from the line and was of deflexed can be explained by concentration polarization theory. It can be concluded that ANN model can well simulate the relationship between permeate flux and TMP at different concentration of NaOH, and the correlation coefficient was up to 0.9997.

As shown in Fig. 10, the ANNs constructed in this study were trained, and the training error curve indicated that the absolute error in the flux was less than 1 after 10000 echo trainings. The training error of retention was less than $10^{-4}$ after 1840 echo trainings. The order of magnitude of the membrane flux is $10^{1}$–$10^{0}$, while that for the retention value ranges from $10^{-2}$ to $10^{-1}$; although the error limits of flux and retention were set differently, the results met our demands for precision.

The ANN prediction of NaOH rejection as a function of flux, along with the experimental data are shown in Fig. 11. As illustrated in Fig. 11, the retention of NaOH increased with increasing flux at fixed concentrations of NaOH, while it decreased with increasing NaOH concentrations at fixed flux. When the NaOH concentration was higher than the highest concentration (about pH 13) the non-anti-alkali membrane could bear, the membrane swelling effect and the effect of ion descreening were enhanced [32], and the electrostatic repulsion effect weakened so that the retention of NaOH by the membrane dropped significantly. Compared to the glucose retention rate, the retention of NaOH by this membrane was very low; the retention difference was about 0.9, even at the low concentrations used in our experiment. This bodes well for applications of the tested membrane system toward the recovery of NaOH. ANN models can accurately simulate the change of retention with flux at different concentration of NaOH, with a correlation coefficient of 0.9918.

As shown in Table 1, the reflection coefficient decreased with increasing concentrations of NaOH, but in the low concentration range (about 1 mol L$^{-1}$ and below) this trend was not apparent. It manifested only in high concentration regimes, especially at about 2 mol L$^{-1}$ and above. This is related to compression of the surface electric double-layer, and the pore size increases. Ps increased from 55.85 L m$^{-2}$ h$^{-1}$ to 431.47 L m$^{-2}$ h$^{-1}$, and this trend followed the decreasing retention. As shown in Fig. 11, the rate of retention increase was decreased with the increasing concentration, as caused by the increase of $P_s$. As shown in Table 1, at each of the experimental concentrations, the correlation coefficients of the SK equation with the experimental values were all greater than 0.98, indicating that the SK equation can accurately simulate the NF system. Compared with the ANN model, the SK equation has a sounder theoretical basis, despite the slightly lower correlation coefficient.

## 5. Conclusions

The results showed that pH strongly affects the membrane flux and solutes retention, and this anti-alkali NF membrane can treat even solutions with high alkali concentrations. The SK model and our ANN model can simulate the performance of nanofiltration. The reflection coefficient of glucose by the membrane σ was 0.9914, the solute permeability $P_s$ was 0.0596 L m$^{-2}$ h$^{-1}$), the membrane pore radius was estimated to be 0.380 nm, and the separation layer equivalent thickness ($\Delta x/A_k$) was 65.63 nm.

Table 1
SK model parameters at different concentration of NaOH

| Concentration (mol L$^{-1}$) | Reflection coefficient | Solute permeability (L m$^{-2}$ h$^{-1}$) | Correlation coefficient |
|---|---|---|---|
| 0.224 | 0.200 | 55.85 | 0.9878 |
| 0.912 | 0.199 | 91.52 | 0.9826 |
| 1.357 | 0.198 | 137.25 | 0.9887 |
| 1.970 | 0.188 | 215.94 | 0.9805 |
| 2.651 | 0.149 | 431.47 | 0.9878 |

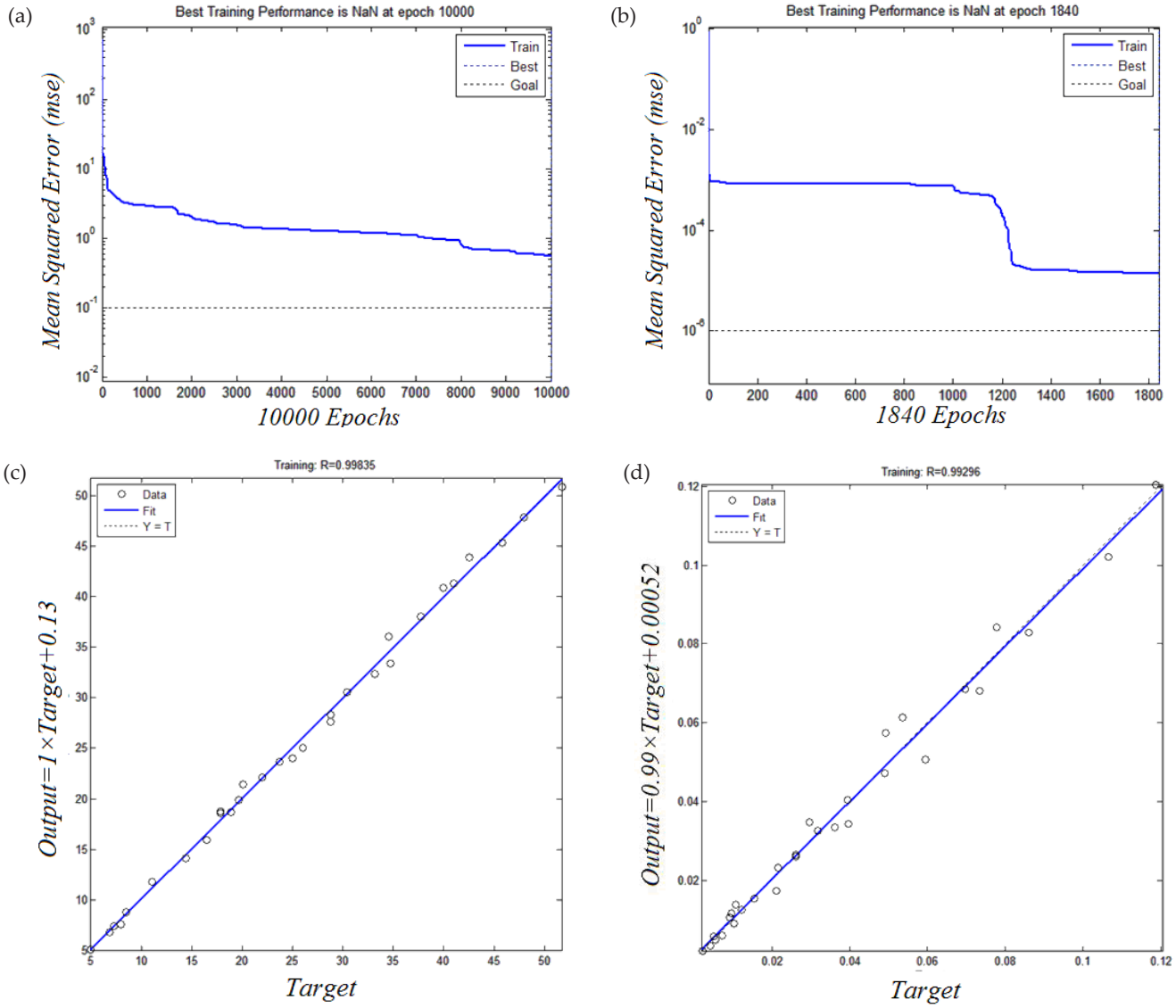


Fig. 10. Training error characteristic curve of ANN model. (a) Flux model training; (b) Retention model training; (c) correlation coefficient of flux between experimental data and simulation data; (d) correlation coefficient of retentration experimental data and simulation data.

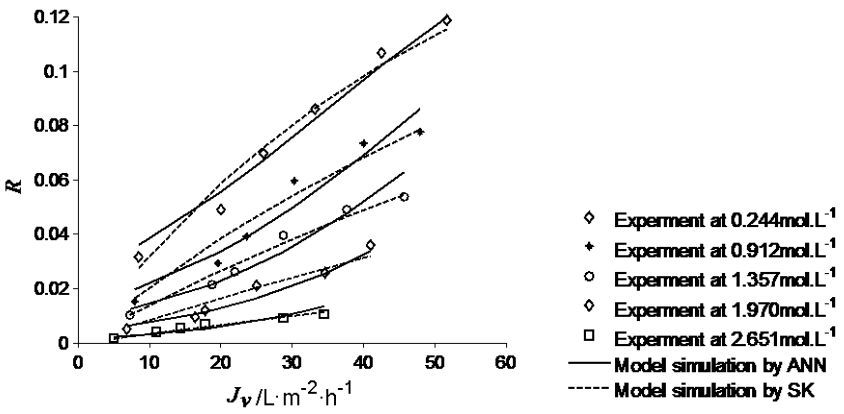


Fig. 11. ANN and SK predictions of rejection of NaOH vs. TMP and NaOH concentration.

The effects of pH on hydrophilicity and surface charge should be investigated in future research, in order to study their effects on the nanofiltration performance of the NF membrane.

## Symbols

$A_m$ — Effective membrane area, $m^2$
$C$ — Solution concentration, $m^{-3}$
$D_s$ — Solute diffusivity, $m^{-2}$ $s^{-1}$
$J_v$ — Permeate flux, L $m^{-2}$ $h^{-1}$
$L_p$ — Pure water permeability, L $m^{-2}$ $h^{-1}$ $bar^{-1}$
$P_{in}$ — Inlet pressure of membrane, bar
$P_{out}$ — Outlet pressure of membrane, bar
$P_s$ — Solute permeability, L $m^{-2}$ $h^{-1}$
$\Delta P$ — Transmembrane pressure,TMP, bar
$R$ — Retention of solute, %
$R_g$ — Ideal gas constant, J $K^{-1}mol^{-1}$
$r_p$ — Theoretical pore radius, m
$T$ — Temperature, K
$\Delta x$ — Membrane thickness, m

*Greek*

$\kappa^{-1}$ — Debye screening length, $m^{-1}$
$\lambda$ — Ratio solute radius to the membrane pore radius
$\mu$ — Dynamic viscosity of solvent, Pa s
$\Delta\pi$ — Osmotic pressure difference, bar
$\sigma$ — Reflection coefficient

## Acknowledgements

This work was financially supported by the National High Technology Research & Development Program of China (863 Program) (No. 2006AA09Z444), and it was also supported by PCSIRT0627and 111 project-B07029. We thank Hyflux (Hydrochem, Shanghai, China) for the equipment support and helpful discussion, and Nantong Shuanglin Chitin Co., Ltd. (Lvsi, Nantong, China) for the raw materials support.

## References

[1] M. Mänttäri, A. Pihlajamäki and M. Nyström. Effect of pH on hydrophilicity and charge and their effect on the filtration efficiency of NF membranes at different pH. J. Membr. Sci., 280 (2006) 311–320.
[2] S. Szoke, G. Patzay and L. Weiser, Characteristics of thin-film nanofiltration membranes at various pH-values, Desalination, 151 (2002) 123–129.
[3] A.E. Childress and M. Elimelech, Relating nanofiltration membrane performance to membrane charge (electrokinetic) characteristics, Environ. Sci. Technol., 34 (2000) 3710–3716.
[4] T. Van Gestel, C. Vandecasteele, A. Buekenhoudt, C. Dotremont, J. Luyten, R. Leysen, B. Van der Bruggen and G. Maes, Salt retention in nanofiltration with multilayer ceramic TiO2 membranes, J. Membr. Sci., 209 (2002) 379–389.
[5] G. Hagmeyer and R. Gimbel, Modelling the rejection of nanofiltration membranes using zeta potential measurements, Separ. Purif. Technol., 15 (1999) 19–30.
[6] G. Hagmeyer and R. Gimbel, Modelling the salt rejection of nanofiltration membranes for ternary ion mixtures and for single salts at different pH values, Desalination, 117 (1998) 247–256.
[7] A.E. Childress and M. Elimelech, Effect of solution chemistry on the surface charge of polymeric reverse osmosis and nanofiltration membranes, J. Membr. Sci., 119 (1996) 253–268.
[8] B. Van der Bruggen, A. Koninckx and C. Vandecasteele, Separation of monovalent and divalent ions from aqueous solution by electrodialysis and nanofiltration, Water Res.. 38 (2004) 1347–1353.
[9] W.R. Bowen, J.S. Welfoot and P.M. Williams, Linearized transport model for nanofiltration: development and assessment, AIChE J., 48 (2002) 760–773.
[10] M. Dornier, M. Decloux, G. Trystram and A. Lebert, Dynamic modeling of crossflow microfiltration using neural networks, J. Membr. Sci., 98 (1995) 263.
[11] E. Piron, E. Latrille and F. René, Application of artificial neural networks for crossflow microfiltration modelling: "black-box" and semiphysical approaches, Comput. Chem. Eng., 21(9) (1997) 1021.
[12] F. Meyer, I. Gehmlic, R. Guthke, A. Gorak and W.A. Knorre, Analysis and simulation of complex interactions during dynamic microfiltration of Escherichia coli suspensions, Biotechnol. Bioeng., 59(2) (1998) 189.
[13] M. Hamachi, M. Cabassud, A. Davin and M.M. Peuchot, Dynamic modeling of crossflow microfiltration of bentonite suspension using recurrent neural networks, Chem. Eng. Process., 38 (1999) 203.
[14] M. Cabassud, N. Delgrange-Vincent, C. Cabassud, L. Durand-Bourlier and J.M. Lainé, Neural networks: a tool to improve UF plant productivity, Desalination, 145 (2002) 223.
[15] G.R. Shetty and S. Chellam, Predicting membrane fouling during municipal drinking water nanofiltration using artificial neural Networks, J. Membr. Sci., 217 (2003) 69.
[16] G.R. Shetty, H. Malki and S. Chellam, Predicting contaminant removal during municipal drinking water nanofiltration using artificial neural networks, J. Membr. Sci., 212 (2003) 99.
[17] N. Delgrange, C. Cabassud, M. Cabassud, L. Durand-Bourlier and J.M. Lainé, Neural networks for prediction of ultrafiltration transmembrane pressure-application to drinking water production, J. Membr. Sci., 150 (1998) 111.
[18] N. Delgrange-Vincent, C. Cabassud, M. Cabassud, L. Durand-Bourlier and J.M. Lainé, Neural networks for long term prediction of fouling and backwash efficiency in ultrafiltration for drinking water production, Desalination, 131 (2000) 353.
[19] W.R. Bowen, M.G. Jones and H.N.S. Yousef, Dynamic ultrafiltration of proteins — a neural network approach, J. Membr. Sci., 146 (1998) 225.
[20] W.R. Bowen, H.N.S. Yousef and J.I. Calvo, Dynamic crossflow ultrafiltration of colloids: a deposition probability cake filtration approach, Separ. Purif. Technol., 24 (2001) 297.
[21] C. Bhattacharjee and M. Singh, Studies on the applicability of artifical neural network (ANN) in continuous stirred ultrafiltration, Chem. Eng. Technol., 25 (2002) 12.
[22] S.M.A. Razavi, S.M. Mousavi and S.A. Mortazavi, Dynamic prediction of milk ultrafiltration performance: a neural network approach, Chem. Eng. Sci., 58 (2003) 4185.
[23] O. Kedem and A. Katchalsky, Permeability of composite membranes, Part I: Electric current, volume flow and flow of solute through membranes. Trans. Faraday Soc., 59 (1963) 1918–1930.
[24] X. Xu and H.G. Spencer, Dye–salt separations by nanofiltration using weak acid polyelectrolyte membranes. Desalination, 114 (1997) 129–137.
[25] B. Andrew, Sulfate removal by nanofiltration, Filtr. Separ., 30 (2001) 18–20.
[26] B. Van der Bruggen and C. Vandecasteele, Removal of pollutants

from surface water and groundwater by nanofiltration: overview of possible applications in the drinking water industry. Environ. Poll., 122 (2003) 435–445.
[27] W. Bowen and H. Mukhtar, Characterisation and prediction of separation performance of nanofiltration membranes. J. Membr. Sci., 112 (1996) 263–274.
[28] H. Al-Zoubi, N. Hilal, N.A. Darwish et al. Rejection and modelling of sulphate and potassium salts by nanofiltration membranes: neural network and Spiegler–Kedem model. Desalination, 206 (2007) 42–60
[29] N. Gradojevic and J. Yang, The application of artificial neural networks to exchange rate forecasting: the role of market microstructure variables, Working Paper 2000-23, Bank of Canada, Ottawa, Ontario, 2000.
[30] C. Aydiner, I. Demir and E. Yildiz, Modeling of flux decline in crossflow microfiltration using neural networks: the case of phosphate removal, J. Membr. Sci., 248 (2005) 53–62
[31] X.L. Wang and N. Shinichi, Permeation performance of nanofiltration membranes for systems of aqueous solutions of neutral solutes with low molecular weight. J. Nanjing Univ. Chem. Technol., 20 (1998) 26–40.
[32] M. Nilsson, G. Trägårdh and K. Ostergren, The influence of pH, salt and temperature on nanofiltration performance. J. Membr. Sci., 312 (2008) 97–106.
[33] V. Freger, Swelling and morphology of the skin layer of polyamide composite membranes: an atomic force microscopy study. Environ. Sci. Technol., 38 (2004) 31–68.